

Impact of PCM type on photocell performance using heat pipe-PCM cooling system: A numerical study

Ramadan Gad* 

Egypt-Japan University of Science and Technology (E-JUST), Energy Resources Engineering Department
Mansoura University, Mechanical Power Engineering Department, Alexandria, Egypt, ramadam.gad@ejust.edu.eg

Hatem Mahmoud 

Egypt-Japan University of Science and Technology (E-JUST), Environmental Engineering Department, Alexandria
Aswan University, Architecture Engineering Department, Aswan, Egypt, hatem.mahmoud@ejust.edu.eg

Shinichi Ookawara 

Tokyo Institute of Technology, Tokyo, Japan, ookawara.s.aa@m.titech.ac.jp

Hamdy Hassan 

Egypt-Japan University of Science and Technology (E-JUST), Energy Resources Engineering Department, Alexandria
Assiut University, Mechanical Power Engineering Department, Assiut, Egypt, hamdy.aboali@ejust.edu.eg

Submitted: 08.08.2022

Accepted: 08.11.2022

Published: 31.03.2023



* Corresponding Author

Abstract: The effectiveness of a hybrid cooling system consisting of flat heat pipes (HP) and a heat sink of phase change material (PCM) for the temperature regulation of the photocell (PV) is studied. The system is mathematically modeled and numerically solved by using MatLab software. The impact of the type of PCM (RT25, RT35, and RT42) in summer on the performance of the hybrid photocell cooling system is analyzed. Results prove that the HP-PCM cooling system performs better than the natural photocell cooling. PCM with a low melting point is more efficient for electric performance than a high melting point. For a given PCM thickness of 4 cm, the maximum temperature of the photocell is reduced by 8.7 °C when PCM RT25 is used as a heat sink compared to 7.5 °C and 7.3 °C for RT35 and RT42, respectively. RT25-based PV/HP-PCM system outperformed a conventionally cooled photocell in terms of electrical efficiency by 5.3%. In comparison, RT35 and RT42 yield incremental gains of 5% and 4.5 %, respectively. As the PCM melting point is lowered, the hourly thermal efficiency increases with a peak of 48.9% for RT25, 33.7% for RT35, and 32.2% for RT42, respectively.

Keywords: Cooling, Heat pipe, Phase change material, Photocell, Thermal efficiency, Thermal storage

Cite this paper
as:

Gad, R., Mahmoud, H., Ookawara S., & Hassan, H., Impact of PCM type on photocell performance using heat pipe-PCM cooling system: A numerical study. *Journal of Energy Systems* 2023; 7(1): 67-88, DOI: 10.30521/jes.1159281

© 2023 Published by peer-reviewed open access scientific journal, JES at DergiPark (<https://dergipark.org.tr/en/pub/jes>)

Nomenclature			
<p>A Area (m^2)</p> <p>C Specific heat capacity ($J/kg \cdot K$)</p> <p>D Width (m)</p> <p>E Energy (J)</p> <p>G Solar radiation (W/m^2)</p> <p>g Gravity acceleration (m/s^2)</p> <p>h film coefficient ($W/m^2 \cdot K$)</p> <p>h_a convective heat transfer coefficient ($W/m^2 \cdot K$)</p> <p>$h_{rad(s-g)}$ radiative heat transfer coefficient ($W/m^2 \cdot K$)</p> <p>h_{fg} Vaporization heat (J/kg)</p> <p>k Thermal conductivity ($W/m^2 \cdot K$)</p> <p>L Length (m)</p> <p>LH Latent heat (J/kg)</p> <p>M Mass (kg)</p> <p>Nu Nusselt number</p> <p>P Power (W)</p> <p>n Normal direction</p> <p>Pr Prandtl number</p> <p>R Thermal resistance (K/W)</p> <p>R_a Rayleigh number</p> <p>T Temperature ($^{\circ}C$)</p> <p>T_{sun} Solar radiation temperature (K)</p> <p>t Time (s)</p> <p>u Velocity (m/s)</p> <p>w groove width (m)</p> <p>w_f groove fin thickness (m)</p> <p>x Thickness (m)</p> <p>ΔT_{vc} Temperature difference between the heat pipe wall and liquid</p> <p>w_a Heat pipe wall</p> <p>w_i Heat pipe wick</p> <p>Abbreviations</p> <p>EVA Ethyl vinyl acetate</p> <p>HP Flat heat pipe</p> <p>HP-PCM Integrated flat heat pipe-phase change material</p> <p>PCM Phase change material</p>	<p>PV Photocell</p> <p>PV/HP-PCM Integrated PV/flat heat pipe-phase change material</p> <p>PVT Photovoltaic thermal</p> <p>TPT Tedlar/PET/Tedlar</p> <p>Greek symbols</p> <p>Δ Difference (change)</p> <p>β Temperature coefficient (k^{-1})</p> <p>θ Inclination angle ($^{\circ}$)</p> <p>δ Groove depth (m)</p> <p>ϵ Emissivity</p> <p>ρ Density ($kg \cdot m^{-3}$)</p> <p>α Absorptivity (%), thermal diffusivity (m^2/s)</p> <p>σ Stefan–Boltzmann constant ($W/m^2 \cdot K^4$)</p> <p>η Efficiency (%)</p> <p>ψ Liquid fraction (%)</p> <p>τ Transmittance</p> <p>μ Dynamic viscosity ($N \cdot s/m^2$)</p> <p>ν Kinematic viscosity (m^2/s)</p> <p>Subscripts</p> <p>a Ambient, Air</p> <p>c Characteristic</p> <p>con Condenser section</p> <p>cond Vapor condensation</p> <p>ev Evaporator section</p> <p>g Glass</p> <p>ins Insulation</p> <p>l Liquid</p> <p>m_1 Melting start point</p> <p>m_2 Melting endpoint</p> <p>rad Radiation</p> <p>ref Reference</p> <p>s Sky, Solid</p> <p>th Thermal</p> <p>v Vapour</p> <p>ve liquid evaporation</p>		

1. INTRODUCTION

The tremendous increase in energy usage, the associated harmful gas emissions, and the dwindling supply of fossil fuels have placed significant pressure on the world to investigate better alternatives. Among the many renewable energy options that have lately emerged as a possible replacement for fossil fuels, solar power stands out as one of the cleanest, most reliable, and least harmful to the environment. Solar panels have been used in various contexts, from producing hydrogen [1] to charging batteries in communication systems to providing electricity for the vast majority of launched satellites since the dawn of these space disciplines [2]. While photocell systems have been commercialized and are widely used, most solar cells convert electricity at roughly 15% – 20% efficiency under optimal working conditions [3]. However, most of the remaining solar radiation is absorbed as heat. Power output is reduced by 0.65% for every one $^{\circ}C$ when the photocells operate under a high temperature [4]. Photocell's excess heat must be removed using appropriate techniques to avoid these unfavorable effects [5]. Researchers are also looking into novel methods to improve the conversion efficiency of photocells. These methods must adhere to strict guidelines, which include being simple to install, inexpensive, and achieving consistent cell temperature distribution.

The researchers have developed numerous strategies for dissipating heat, which can be divided into passive and active cooling modes. Unlike the passive cooling mechanism, pumps or fans are used in active cooling systems to power the flow of cooling fluid. Water, air, and oil flow are simple and natural ways to accomplish active cooling; however, the non-uniform cooling effect results from increased cell temperature in the direction of fluid flow [6]. The non-uniform temperature pattern would cause

structural failure and low conversion efficiency because of the long-term presence of thermal stress. Uniform cooling using heat sinks and spreaders, phase change materials, and heat pipes are cooling techniques used to avoid these adverse effects [7]. Generally, active cooling, on the whole, is more expensive and more complicated than passive cooling, but it is more efficient [8].

PCMs can transfer much heat during phase transitions, making them ideal for use in applications requiring large amounts of heat to be transferred. In addition to their use in air conditioning cycles [9–11], PCMs also used in recycling waste heat and thermal storage [12,13]. Recently, PCMs have witnessed much investigation in the field of solar power generation due to their high phase change enthalpy, ease of use, low cost, chemical stability, and usable phase transition temperature [14]. The coupling of photocells with phase change material (PV/PCM) cooling has increased in popularity [15]. Since PCM is assimilated at the photocell back, the surplus heat created by the photocell can be absorbed by the PCM, maintaining the photocell temperature at a satisfactory level and approximately uniform for a long time during the thermal regulation. Moreover, it does not require heat transfer fluids or moving parts, as other active cooling systems do. When the photocell panel's operating temperature exceeds the PCM's melting point during sunny hours, the PCM heat sink absorbs heat from the photocell. PCMs are chosen based on their thermophysical properties, including a high latent heat capacity and thermal conductivity with a melting point within the range of the photocell operating temperature. To control the temperature of the photocell, [16] employed two different PCM materials. The maximum operating temperature of the photocell, which was cooled using PCM, was reduced by 6.4 °C and 7.5 °C, respectively, when RT27 and RT31 were utilized as opposed to the photocell alone. In addition, RT31's electric efficiency grew by 4.19%, whereas RT27's electric efficiency increased by only 2.86%. They ultimately determined that 0.34 kg/m² of PCM was required to reduce the photocell temperature by one °C; however, the quantity of PCM required varied according to the PCM's characteristics. The impact of PCM melting point and thickness was studied by [17]. They created a simulation analysis to examine PCM's effect on the photocell system's performance. In the summer simulation, PCMs of melting points from 26 to 30 °C and thicknesses from 3 to 5 cm were investigated, whereas PCMs of melting points from 16 to 18 °C were employed for the winter simulation. Compared to using just one type of PCM, the photocell's thermal regulation lifespan is extended when multiple layers are employed in an appropriate arrangement and design [18].

While the PV/PCM method for photocell thermal regulation wastes thermal energy stored in PCMs, the PVT method allows the thermal energy generated by solar cells to be retrieved and used in other heating systems. Diverse configurations and designs for PVT/PCM systems have been proposed. The most significant advantage of PVT systems is that they provide electric and thermal energy for a minimal additional cost and a fraction of the space is required in this respect. The PV/PCM module's electric output power was improved by utilizing a thermoelectric generator [19]; thereby, electricity could be generated at night, too. They reported a 20 °C reduction in the temperature of cells. Using natural water, the study [20] demonstrated a hybrid PVT system that extracts heat from a PCM attached directly behind a PV panel. Constant water flow from top to bottom has proven to be the most effective design. Compared to the traditional photocell, the achievable configuration reduced operating temperatures by 5.4 °C while increasing electric output by 11.9%, electric efficiency by 12.4%, and overall efficiency by 26%. Carmona and co-workers also worked in this general field (PVT), but they used a modified hybrid PVT system coupled with PCM as the thermal storage to draw attention to the flaws in some previously reported modules [21].

The primary disadvantage of PCMs is their poor thermal conductivity, which slows the heat transfer rate and restricts their use. However, heat pipe (HP) is superior in its capacity to transfer heat at fast rates in a constrained space over extended distances with a low-temperature gradient. The heat pipe consists of three main parts: The evaporator section (attached to the heat source), the adiabatic section, and the condenser section (attached to the heat sink). In the evaporator, the HP working fluid evaporates as it comes into direct contact with the heat source. Following its path through the adiabatic region, the vapor enters the condenser, which cools and gives its latent heat to the heat sink. HP provides high thermal performance, manageable control and construction, a compact structure, and the capability to adapt to various layout circumstances. Some studies used heat pipes as a cooling technique to regulate the cell

temperature [22,23]. They also used active cooling to extract the heat from the condenser section, which reduces the overall system efficiency due to the power used in active cooling. However, using heat pipes as a cooling method for photocells is inefficient as the extracted heat is not utilized, which means low overall system efficiency. Recently some researchers have involved HP in PVT systems to attain significant enhancement in thermal gain and electric output [24–28]. The poor thermal conductivity of PCM might be overcome by using HPs as an intermediate element between the heat source and the PCM storage system, where HPs could be utilized. In this configuration where PCM is used as an indirect heat sink, the PCM-assisted heat pipe module has additional advantages, including temperature regulation, separating the heat source and sink, enhancing PCM's performance by controlling the PCM amount, and increasing the heat transfer rate from the photocell via using super conductor device (heat pipes) and dissipates this heat through a larger area (control the condenser section). Several studies have promoted heat pipes combined with PCM as a cooling method for electronics [29–31] and a battery cooling system for electric vehicles [32–34]. Sweidan et al. [35] suggested a transient numerical model for optimizing the operation of a PVT system coupled with a heat pipe/water/PCM. They used PCM as a cylindrical tube placed inside a water tank to absorb heat from the condenser section. In this system, a portion of heat from the heat pipe is absorbed by the water tank, and the rest of the heat is stored in the cylindrical tubes of PCM. Finally, they show that the best volume of the storage tank for a 4 kW power output is 0.037 m³ and needs a PCM amount of 22.42 kg.

According to previous works of literature, to compensate for the PCM's low thermal conductivity and difficulty controlling the amount of PCM in the case of the direct PCM-heat sink (PV-PCM) cooling system, heat pipes can be installed to transfer heat from the heat source far away to the heat sink, allowing for the cooling of various thermal systems (such as batteries and electronics). However, there has been very little research into the possibilities of hybrid PCM-assisted heat pipe systems as an indirect heat sink for photocell cooling. As a result, the current work analyses the theoretical performance of a hybrid cooling system composed of HP-PCM for the thermal management of photocells (PV/HP-PCM). Also, three PCMs' melting temperature impact on the photocell performance is analyzed and reported. The photocell module heats the heat pipe evaporator while the PCM cools the condenser. The photocell analyses are explored by using three PCMs, namely RT25, RT35, and RT42, for summer under Egypt's climate conditions. The experimental and theoretical results from the past are used to validate the model outcomes of the transient mathematical model. The suggested hybrid cooling system's effects on the photocell temperature, photocell energy efficiency, photocell electric power output, PCM thermal behavior, and PCM thermal efficiency are detailed. This work is significant because it passively extracts heat from the photovoltaic system via a superconductor device (flat heat pipe), requiring no power or maintenance. More importantly, as opposed to making direct contact with the PCM, the proposed cooling method boosts photocell output by increasing the heat extracted from the photocell via controlling the heat transfer area (condenser area) and a more straightforward system setup by controlling the quantity of PCM. This paper presents these points to the authors' best survey that were not considered before. Firstly, the impact of using the hybrid cooling system of flat heat pipe/phase change material (indirect PCM cooling) for thermal management of photocell under hot climate conditions. Secondly, the impact of the melting point change of PCM on the photocell thermal and electric performance.

The proposed cooling system (PV/HP-PCM) is described from two aspects. Firstly, the physical model shows a schematic diagram of the proposed cooling system. Each part of the cooling system is described in terms of its function and configuration. Secondly, the mathematical model, which contains the governing equation, is developed to predict the performance of the proposed cooling system. In this section, energy balance equations are applied for the current model's main parts: Photocell model, heat pipe model, and PCM model. Finally, the mathematical model solving shows the performance of the proposed system under studied parameters.

2. PHYSICAL MODEL

The PV/HP-PCM model consists of three main components as shown in Fig. 1(a,b): Photocell panel (glass, upper encapsulated ethyl vinyl acetate (EVA), silicon cell (polycrystalline silicon), lower EVA, and back Tedlar/PET/Tedlar (TPT) layer). HP (which has three sections namely evaporator, adiabatic, and condenser section), and PCM container. The heat pipe's evaporator part is attached to the back of the photocell and is used to transfer heat generated by the photocell to the heat sink. By evaporating the working fluid within the heat pipe's container core, heat is transferred from the evaporator to the condenser section, as shown in Fig. 1(b,c). The thermal energy is transferred to the PCM-Heat sink via condensation in a condenser section, which is placed under the PCM heat sink, as shown in Fig. 1(d). The system's entire width is 0.2 m, while the length of the evaporator is 0.2 m (matching the length of the solar cell) and the length of the condenser section is 0.25 m (matching the length of the PCM-Heat sink container). This study uses three different PCMs namely RT25, RT35, and RT42. The quantity of PCM is often represented by its thickness in PCM. Each layer of PCM is 0.05 mm thick, and the overall PCM thickness is calculated using the optimal amount of each PCM type. The heat pipe evaporator section makes the angle of θ form the horizontal plane. The properties of PV/HP/PCM system: PCM (melting range, thermal conductivity, latent heat, density, and specific heat), heat pipe and inside working fluid (dimensions and thermophysical properties of heat pipe materials and working fluid), are listed in Table 1, while the thermophysical and optical properties of photocell layers (absorptivity, transmissivity, and emissivity) are listed in Table 2.

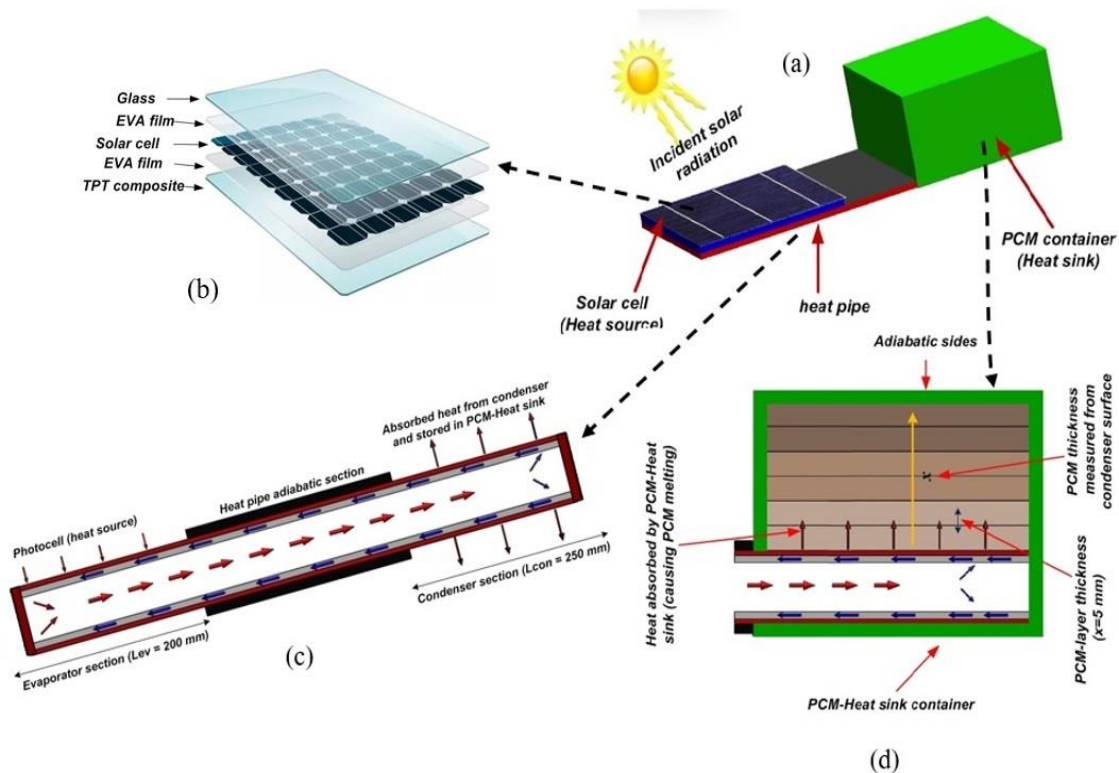


Figure 1. Schematically presentation of the proposed design of a PV/HP-PCM system: Three main components: (a) Photocell layers, (b,c) flat heat pipe with its three sections, and (d) PCM-heat sink.

Table 1. Physical and thermal properties of PCMs, heat pipe, and working fluid inside heat pipe [36–38].

Thermophysical properties	RT42	RT35	RT25	Heat pipe	Working fluid of HP
Cp (J/kg.K)	2000	2000	2000	900	-
K (W/m.K)	0.2	0.2	0.2	230	0.168
ρ_{solid} (kg/m ³)	0.2	148	677	2700	2.37 (vapor)
ρ_{liquid} (kg/m ³)	0.3	0.15	1250	-	744
Melting point (°C)	37/43	29/35	25/26	-	-
Heat of fusion (kJ/kg)	165	160	180	-	518

Table 2. The dimensions of the photocell layer, thermal, and optical properties [39].

Thermophysical properties	Photocell layers			
	Glass	EVA	Silicon	TPT
Cp (J/kg.K)	500	2090	677	1250
K (W/m.K)	2	0.311	148	0.15
ρ (kg/m ³)	2450	960	2330	1200
Transmissivity	0.91	0.9	-	-
Absorptivity	0.04	0.08	0.9	-
emissivity	0.85	-	-	0.9
Thickness (mm)	3.2	0.5	0.2	0.3

3. MATHEMATICAL MODEL

The proposed module's performance and temperature regulation are studied by using the transient energy balance equation. This model aims to assess the parameters affecting the solar panel's performance, such as PCM type (melting range) on the thermal performance (operating temperature) and electric performance (electric efficiency and electric power) of the photocell. Furthermore, PCM type impacts PCM's thermal performance (average PCM temperature, melting fraction, average PCM efficiency, and thermal energy storage in PCM). The governing equations of the proposed cooling system are divided into three sections: The photocell model, the heat pipe model, and the thermal model of PCM.

3.1. Photocell Model

As shown in Fig. 1(b), the polycrystalline silicon is encased in an ethyl vinyl acetate (EVA) layer on the upper layer of the PV panel, followed by an EVA layer on the lower layer with glass and TPT as the first and lower layer, respectively. Following energy balance equations for each component of the photocell are written as follows:

3.1.1. Glass cover

The change in the temperature of each layer with time is shown as follows:

$$m_g C_g \frac{\partial T_g}{\partial t} = G A_g \alpha_g - h_a A_g (T_g - T_a) - h_{rad(s-g)} A_g (T_g - T_s) - \frac{T_g - T_{EVA1}}{R_{g-EVA}} \quad (1)$$

where $m_g C_g$, A_g are the mass, heat capacity, and area of the glass layer. The left term in Eq. (1) represents the transient change in glass layer temperature, while the first right-hand term represents the amount of solar radiation absorbed by the glass. The heat transfer convective (h_a), which is a function of wind velocity (u_a), and radiative ($h_{rad(s-g)}$) coefficients for the first photocell layer (i.e. glass layer) represent the amount of heat lost to the ambient by convection and conduction and are calculated as follows [40]:

$$h_a = 5.82 + 4.07 u_a \quad (2)$$

$$h_{rad(s-g)} = \varepsilon_g \sigma (T_g^2 + T_s^2) (T_g + T_s) \quad (3)$$

T_s is the sky temperature, with $T_s = 0.037536 T_a^{1.5} + 0.32 T_a$, with T in K while T_a and T_g are ambient and glass temperature, respectively. The last term in Eq. (1) represents heat transfer by conduction from the glass layer to the upper EVA layer.

3.1.2. Upper EVA layer

The transient change in the temperature of the EVA layer with time is shown as,

$$m_{EVA} C_{EVA} \frac{\partial T_{EVA1}}{\partial t} = G A_{EVA} \alpha_{EVA} \tau_g + \frac{T_g - T_{EVA1}}{R_{g-EVA}} - \frac{T_{EVA1} - T_{pv}}{R_{SC-EVA}}. \quad (4)$$

The first right-hand term represents the amount of solar radiation that passes through the glass and is absorbed by the EVA layer, while the last two terms are heat transferred by conduction.

3.1.3. Photocell silicon layer (SC)

The silicon layer time-dependent temperature variation is computed by:

$$m_{SC} C_{SC} \frac{\partial T_{pv}}{\partial t} = G A_{SC} \alpha_{SC} \tau_g \tau_{EVA} - P_{SC} + \frac{T_{EVA1} - T_{pv}}{R_{SC-EVA}} - \frac{T_{SC} - T_{EVA2}}{R_{SC-EVA}}. \quad (5)$$

The first right-hand term is the amount of solar radiation that passes through the first two layers (i.e. glass and EVA) and is absorbed by the silicon layer, while the second term is the instantaneous electric power of the photocell and is governed by [41]:

$$P_{SC} = A_{SC} G \alpha_{SC} \tau_g \tau_{EVA} \eta_{SC}. \quad (6)$$

The photocell efficiency, which is a function of photocell operating temperature and reference efficiency, is formulated using [37,42]:

$$\eta_{SC} = \eta_{ref} \left(1 - \beta_{SC} (T_{SC} - T_{ref}) \right) \quad (7)$$

The reference efficiency of photocell η_{ref} is assumed to be 15% at a reference temperature T_{ref} of 298 K and β_{SC} equal 0.0045 k^{-1} [39].

3.1.4. Lower EVA layer

The energy equation for the last two layers contains conduction heat transfer as no solar radiation passes through the silicon layer.

$$m_{EVA} C_{EVA} \frac{\partial T_{EVA2}}{\partial t} = \frac{T_{SC} - T_{EVA2}}{R_{SC-EVA}} - \frac{T_{EVA2} - T_{TPT}}{R_{TPT-EVA}} \quad (8)$$

3.1.5. TPT layer

The transient change in the temperature of the last layer of the photocell with time is shown as,

$$m_{TPT} C_{TPT} \frac{\partial T_{TPT}}{\partial t} = \frac{T_{EVA2} - T_{TPT}}{R_{TPT-EVA}} - \frac{T_{TPT} - T_{ev}}{R_{ev-TPT}} \quad (9)$$

The resistance (R) between any two photocell layers (glass and EVA layer (R_{g-EVA})), EVA and silicon layer (R_{pv-EVA}), and EVA and TPT layer ($R_{TPT-EVA}$), and TPT and heat pipe evaporator (R_{ev-TPT}) is conduction resistance calculated by Eq.(10).

$$R = \frac{1}{2} \left[\left(\frac{x}{kA} \right)_{upper} + \left(\frac{x}{kA} \right)_{lower} \right] \quad (10)$$

Where x , k , and A are the thickness, thermal conductivity, and area of each layer.

3.2. Heat Pipe Model

The heat pipe thermal model is a sum of series resistances R_{con-ev} from the evaporator to the condenser section [43].

$$R_{con-ev} = R_{ev-ve} + R_{ev-wi} + R_{ev-wa} + R_{con-cond} + R_{con-wi} + R_{con-wa}. \quad (11)$$

The following equations show in detail the definition of each term in the equation above. The resistance of liquid evaporation inside the evaporation section is given by,

$$R_{ev-ve} = \frac{1}{L_{ev} D_{ev} h_{ev}}, \quad (12)$$

where L_{ev} and D_{ev} are the evaporator length and width, respectively. The film coefficient (h_{ev}) is given as follows [44]:

$$h_{ev} = \frac{k_l}{x_{ev-wi}}, \quad (13)$$

where k_l is the thermal conductivity of the heat pipe liquid, and x_{ev-wi} is the thickness of the evaporator wick. The conduction resistance inside the wicked metal of the evaporation and condenser sections are given below, respectively:

$$R_{ev-wi} = \frac{x_{ev-wi}}{k_{wi} L_{ev} D_{ev}}, \quad (14)$$

$$R_{con-wi} = \frac{x_{con-wi}}{k_{wi} L_{con} D_{con}} \quad (15)$$

The grooved wick thermal conductivity is calculated as follows [43]:

$$k_{wi} = \frac{w k_l [(0.185 k_{wa} w_f + \delta k_l) + (\delta k_l k_{wa} w_f)]}{[(w + w_f) [(0.185 k_{wa} w_f + \delta k_l)]]}, \quad (16)$$

where w , δ , and w_f are the groove width, depth of the groove, and groove fin thickness, respectively. k_{wa} is the heat pipe wall thermal conductivity, respectively. The wall thermal resistances for the evaporator, and condenser section, are defined as follows:

$$R_{ev-wa} = \frac{x_{ev-wa}}{k_{wa} L_{ev} D_{ev}}, \quad (17)$$

$$R_{con-wa} = \frac{x_{con-wa}}{k_{wa} L_{con} D_{con}} \quad (18)$$

where L_{con} and D_{con} are the condenser section length and width, respectively. x_{ev-wa} and x_{con-wa} are the heat pipe wall thickness at the evaporator and condenser section, respectively. The resistance of vapor condensation inside the condenser section due to heat absorbed from the condenser to the PCM-heat sink is given as follows [45]:

$$R_{con-cond} = \frac{1}{L_{con}D_{con}h_{cond}} \quad (19)$$

The film condensation (h_{cond}) is given below by following [46]:

$$h_{cond} = 1.13 \left[\frac{g \sin(\theta) \rho_l (\rho_l - \rho_v) k_l^3 h_{fg}}{\mu_L \Delta T_{vc} L_{con}} \right]^{0.25}, \quad (20)$$

where ρ_l and ρ_v are the liquid and vapor densities of heat pipe liquid, respectively while μ_L and h_{fg} are the dynamic viscosity and heat of fusion of the liquid inside the heat pipe, respectively. θ is the system's inclined angle and ΔT_{vc} is the temperature difference between the heat pipe wall and the inside liquid.

3.2.1. Evaporator section

The heat pipe evaporator section absorbs excess heat from the back surface of the PV panel, part of this heat is lost to the ambient by convection, and the rest is transported to the condenser. The mathematical equation (energy balance) of the evaporator:

$$m_{ev} C_{HP} \frac{\partial T_{eva}}{\partial t} = \frac{T_{TPT} - T_{ev}}{R_{ev-TPT}} - \frac{T_{ev} - T_{con}}{R_{con-ev}} - \frac{T_{ev} - T_a}{R_{ev-a}}, \quad (21)$$

where R_{ev-a} represents the convective resistance from the evaporator and the ambient.

$$R_{ev-a} = \frac{1}{h_{ev-a} L_{ev} D_{ev}}, \quad (22)$$

$$h_{ev-a} = \frac{Nu_{ev-a}}{L_{ev}} k_a \quad (23)$$

where h_{ev-a} is the convective heat transfer coefficient between the back side of the heat pipe evaporator section and the ambient. For the laminar flow, the Nusselt number is calculated as follows [47]:

$$Nu_{ev-a} = \left[0.825 + \frac{0.387 Ra_a^{1/6}}{[1 + (0.492/Pr_a)^{9/16}]^{8/27}} \right]^2 \quad (24)$$

$$Ra_a = \frac{g \cos(\theta) B (T_{ev} - T_a) L_c^3}{\nu \alpha} \quad (25)$$

where ν and R_a are kinematic viscosity and Rayleigh number of air, $B = 2/(T_{ev} + T_a)$, α_a is the air thermal diffusivity, $\alpha_a = \frac{k_a}{\rho_a C_a}$. Pr_a is Prandtl number of air following [47]:

$$Pr_a = \frac{\mu_a C_a}{k_a}, \quad (26)$$

where μ_a , C_a , and k_a are the dynamic viscosity, specific heat, and thermal conductivity of air, respectively.

3.2.2. Condenser section

The thermal model of the condenser section takes into account two thermal resistances: The conduction with PCM ($R_{con-pcm}$) and a sum of series resistances with the evaporator section (R_{con-ev}), as listed below:

$$m_{con} C_{HP} \frac{\partial T_{con}}{\partial t} = \frac{T_{ev} - T_{con}}{R_{con-ev}} - \frac{T_{con} - T_{pcm}}{R_{con-pcm}}, \quad (27)$$

the conduction resistance $R_{con-pcm}$ between the condenser and the first layer of PCM, which is defined as,

$$R_{con-pcm} = \frac{1}{2} \left(\left(\frac{x}{kA} \right)_{con} + \left(\frac{x}{kA} \right)_{pcm} \right). \quad (28)$$

3.3. Energy Balance of PCM

Since PCM is described by low thermal conductivity, PCM amount (thickness) significantly impacts the PCM model's solution. The PCM total thickness is considered multi-small thickness (layers), and the symbol x represents each layer's thickness measured from the condenser section. The PCM's energy balance of each layer is described as follows [36]:

$$x_{pcm} \rho_{pcm} C_{pcm} \frac{\partial T_{pcm}}{\partial t} = k \frac{\partial T}{\partial x}. \quad (29)$$

For the first layer:

$$k \frac{\partial T}{\partial x} = \frac{T_{con} - T_{pcm1}}{R_{con-pcm1}} - \frac{T_{pcm1} - T_{pcm2}}{R_{pcm}}. \quad (30)$$

For the intermediate layers:

$$k \frac{\partial T}{\partial x} = k_{pcm} \frac{\Delta T_{pcm}}{\Delta x_{pcm}}. \quad (31)$$

For the last layer (n):

$$\frac{\partial T}{\partial x} = \frac{T_{pcm,n-1} - T_{pcm,n}}{R_{pcm}} - \frac{T_{pcm,n} - T_a}{R_{pcm-a}}, \quad (32)$$

where R_{pcm-a} is the resistance between the last layer and the surrounding is given by,

$$R_{pcm-a} = \left(\frac{x}{2k} \right)_{pcm} + \left(\frac{x}{k} \right)_{ins} + \frac{1}{h_a}. \quad (33)$$

3.4. Thermo-physical Properties of PCM

Because the proposed hybrid cooling model's performance depends on PCM's properties, it is critical to employ suitable PCM, particularly thermo-physical properties [48].

3.4.1. Density

The density of PCM depends on the phase change process as follows [49]:

$$\rho_{pcm} = \begin{cases} \rho_{pcm,s} & T_{pcm} \leq T_{m1} \\ \psi\rho_{pcm,l} + (1 - \psi)\rho_{pcm,s} & T_{m1} < T_{pcm} \leq T_m \\ \rho_{pcm,l} & T_{pcm} > T_{m2} \end{cases} \quad (34)$$

The PCM melting rate (ψ) is calculated using Eq. (35) as follows [50]:

$$\psi = \frac{T_{pcm} - T_{m1}}{T_{m2} - T_{m1}} \quad (35)$$

where $T_m = \frac{T_{m1} + T_{m2}}{2}$, T_{m1} and T_{m2} are melting range of PCM (start and end melting temperatures).

3.4.2. Thermal conductivity

During the phase transition process, the PCM thermal conductivity is changed in the following way [49]:

$$k_{pcm} = \begin{cases} k_{pcm,s} & T_{pcm} \leq T_{m1} \\ \psi k_{pcm,l} + (1 - \psi)k_{pcm,s} & T_{m1} < T_{pcm} \leq T_m \\ k_{pcm,l} & T_{pcm} > T_{m2} \end{cases} \quad (36)$$

3.5. Thermal Energy Storage in PCM

Hourly PCM energy storage (E_{th}) is the amount of heat absorbed sensibly and latently during the photocell thermal regulation and is defined as [36]:

$$E_{th} = \begin{cases} m_{pcm}c_{pcm,s}(T_{pcm,t} - T_{pcm,t_o}), & T_{pcm} \leq T_{m1} \\ (1 - \psi)m_{pcm}c_{pcm,s}(T_{pcm,t} - T_{pcm,t_o}) + \Delta\psi m_{pcm}H, & T_{m1} < T_{pcm} \leq T_{m2} \\ (1 - \psi)m_{pcm}c_{pcm,s}(T_{pcm,t} - T_{pcm,t_o}) + \Delta\psi m_{pcm}H \\ + \psi m_{pcm}c_{pcm,l}(T_{pcm,t} - T_{pcm,m}), & T_{pcm} > T_{m2} \end{cases} \quad (37)$$

In this study, PCM's thermal efficiency is calculated according to Eq. (38) and defined as the amount of energy storage in PCM to the amount of solar energy incident on the PV cell.

$$\eta_{th} = \frac{E_{th}}{GA_{pv}t} \quad (38)$$

3.6. Initial and Boundary Conditions

Ambient temperatures are considered for the initial temperatures of the PV /HP/PCM. The PCM is considered to have a higher starting temperature than the nighttime temperature in this study. As revealed in Fig. 1(d), the PCM container is insulated as follows:

$$\frac{\partial T}{\partial n} = 0, \quad (39)$$

where n is the normal direction. The evaporator's lower surface is a convective boundary, given as follows [51]:

$$-k \frac{\partial T}{\partial n} = h_a(T_{ev} - T_a). \quad (40)$$

The upper layer of the photocell glass is exposed to convection and radiation as follows [52]:

$$-k \frac{\partial T}{\partial n} = h_a(T_g - T_a) + h_{rad(s-g)}(T_g - T_s). \quad (41)$$

The photocell's upper and lower boundary conditions are identical to the PV/HP/PCM system.

4. MODEL VALIDATION

To validate the numerical results of the photocell and PV/PCM system, the validation of homemade program code, which is solved and analyzed using MatLab 2021b software, is realized in two steps: First, validation with the theoretical results of the photocell model [39], which is cooled from the top and bottom surfaces by convection and radiation. Second, validation with the results of [53], which conducted experimental work for cooling the photocell using PCM as a heat sink.

Initially, the present model cell temperature is compared with the results of [39]. Fig. 2 compares the temperature difference between the photocell and ambient temperature of current work and that of [39] at different solar radiation from 200 W/m² to 1000 W/m².

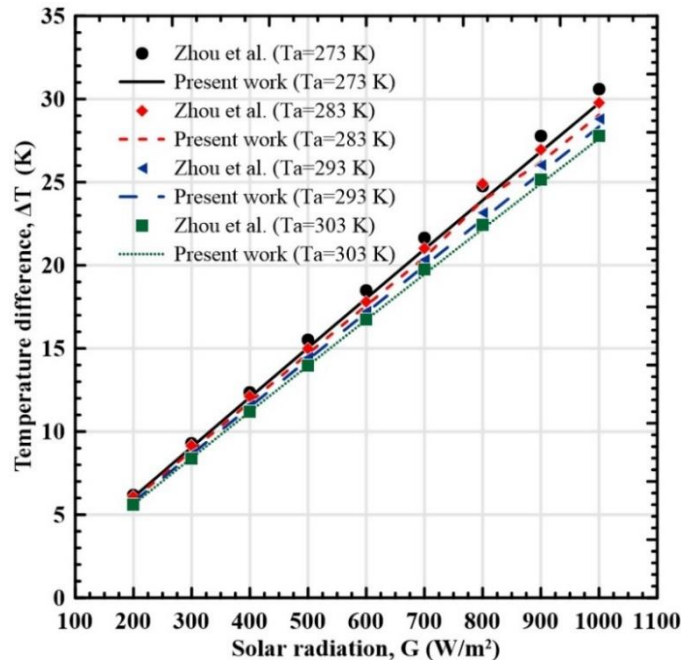


Figure 2. The current model results for different solar radiation compared with Zhou et al. [39].

According to the graph, findings from the present photocell model are in good agreement with the numerical results. Secondly, the predicted results from the current work were validated with the experimental data of [53] by studying the average temperature of the PV/PCM system during the day, as illustrated in Fig. 3.

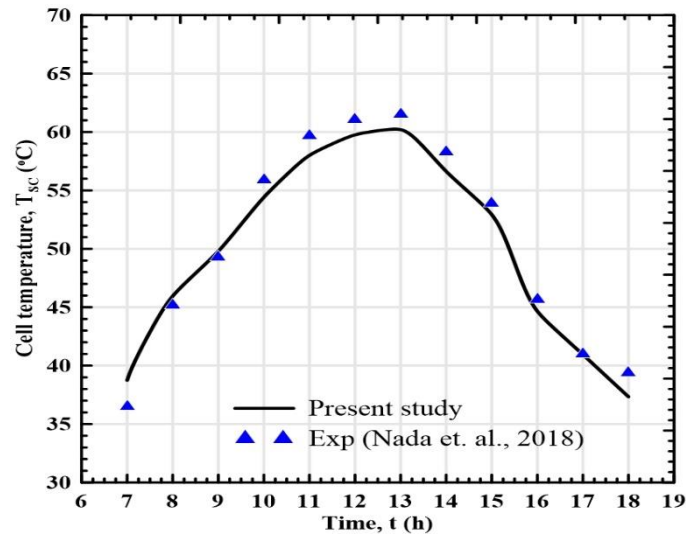


Figure 3. Predicted average photocell temperature of the present work with the measured values of Nada et al. [53].

In this validation, PCM and paraffin wax RT55, were used as a heat sink for heat generated by photocell. The experiments were conducted outdoors, and PCM was contained in galvanized sheet container. The validation's maximum error is about 5.5 % (i.e. 2.2 °C difference between the results).

5. RESULTS AND DISCUSSION

The results are presented for climate conditions on the 5th of August for summer conditions for Assuit city, Egypt. In this study, the length of the evaporator, adiabatic, and condenser sections of the heat pipe are 0.25 m, 0.05 m, and 0.2 m, respectively, and a total width of 0.2 m. The PCM thickness is used to represent the quantity of the PCM. Three PCM are selected based on their melting range i.e. RT42 with a high melting range (37-42 °C), RT25 with a low melting range (25-26 °C), and RT35 with a melting range of ((29-35 °C). The cooling system's performance with PCM is compared with photocell under free air cooling without using HP and PCM (conventional photocell). Fig. 4 illustrates the studied climate conditions vary with time: The solar radiation, wind speed, and ambient temperature.

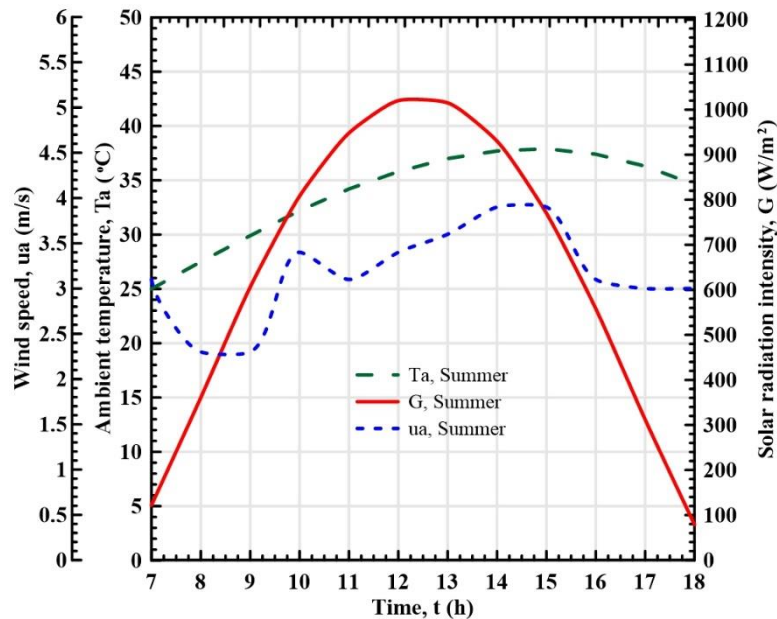


Figure 4. Variation of the studied ambient condition with time.

5.1. PCM Performance

5.1.1. PCM temperature

Fig. 5 shows the average PCM temperature variation with time of RT42, RT35, and RT25 at 4 cm thickness. In the first period, PCM absorbs the heat dissipated from the photocell via the condenser section sensibly. After that, PCM starts to melt as the heat transfer rate to PCM increases.

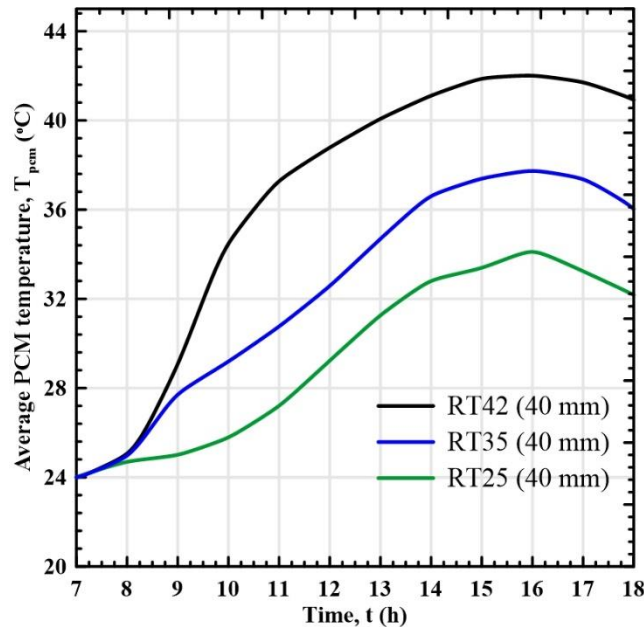


Figure 5. Average temperature variation of PCM layers with time.

During this period, the change in the temperature of PCM is small. The temperature of the PCM then increases sensibly after complete melting. For example, RT35 absorbs sensible heat, as apparent in Fig. 5 case RT35 (from 24 °C to 27.7 °C). After that, PCM goes phase change transition (the temperature of RT35 lies in its melting range from 29 °C at 10:00 AM to 34.6 °C at 13:00). After a significant amount of RT35 is melted, RT35 absorbs most of the heat sensibly (RT35 average temperature higher than the upper melting point). It is also noted that RT42 melts partially, where the average temperature, after the sensible heating period, is in the range of its melting range (from 37.2 °C at 11:00 AM to 41 °C at 18:00). Fig. 5 illustrates that the average temperature of PCMs is a function of their melting range (the temperature of RT42 is higher than RT35 and RT25). This means the operating temperature of the photocell is close to the average temperature of the PCM. From these results, the PCM melting point significantly affects the operating temperature of the photocell, as will be shown later.

5.1.2. PCM liquid fraction

The change of PCM liquid fraction percentages for different PCM types is shown in Fig. 6. It is clear that PCM liquid fraction increases with decreasing PCM melting point for the same amount of PCM. The increase in liquid fraction maximizes cell temperature reduction. The results of Fig. 6 depict that the liquid fraction of RT25 is higher than RT23 and RT42, which means more heat is absorbed by the hybrid cooling system using RT25. In this study, the same amount of PCM (4 cm thickness above the condenser section) is used for RT42, RT35, and RT25. This amount is selected based on RT25 (the PCM type that achieved the lowest photocell operating temperature).

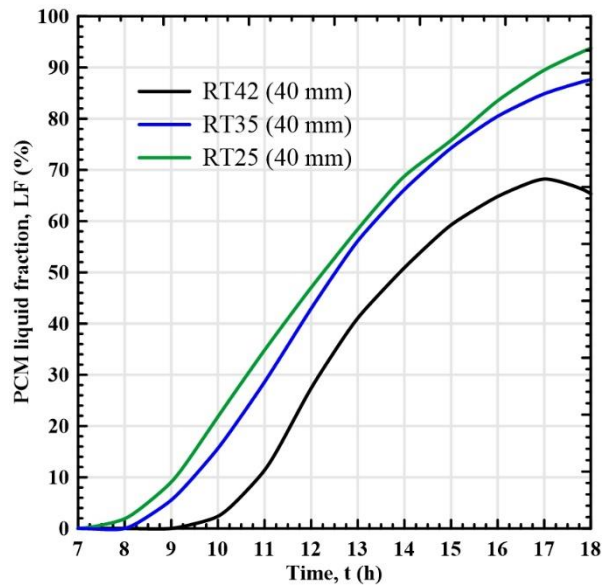


Figure 6. Variation of PCM liquid fraction with time.

As shown in Fig. 6, about 93.7% of RT25 is melted by the end of the day, and this melted amount of RT25 is higher than the value of other PCMs. The increase in the melting rate for RT25 is because RT25 has a low melting range (25-26 °C) compared with other PCM types. Increasing the PCM melting temperature (more time is needed to melt PCM completely) decreases the amount of PCM required (RT35 and RT24 have final liquid fractions of 87.6 % and 65.3%, respectively). As a result, the photocell system needs a large amount of PCM with a low melting point (RT25), and the system needs more time during the day to solidify PCM. On the other hand, the cooling system needs less PCM with a high melting point, which means a lighter and more economic system; besides, less time is required for night PCM cooling. However, PCM with a high melting point has a high photocell operating temperature compared with a low melting point.

It is remarked that for RT42, at the end of the day, the melting rate decreases again. Because in the afternoon, solar intensity decreases, resulting in less heat generated by the photocell, thereby heat generated from the photocell is lower than the amount of heat stored in PCM. That results in heat flow from the PCM to the photocell and increases the system cell temperature greater than the conventional photocell cooling. This backflow heat reduces the percentage of liquid fraction, as depicted in Fig. 6 case RT42.

5.1.3. PCM efficiency

The thermal efficiencies of RT25, RT35, and RT42 are depicted in Fig. 7. The PCM thermal efficiency is defined by Eq. 38. According to this definition, PCM efficiency grows with time as solar radiation increases. After that, the efficiency decreases as the heat generated by the photocell decrease (solar radiation decreases). As stated before, the negative value of thermal efficiency is due to the heat transferred from the PCM to the photocell, as shown in Fig. 7 case RT42. It is also noted that the maximum thermal efficiency of the different PCMs is not achieved at noontime; however, maximum energy is generated from the photocell because a large amount of PCM is melted. The PCM type has a considerable impact on PCM thermal efficiency.

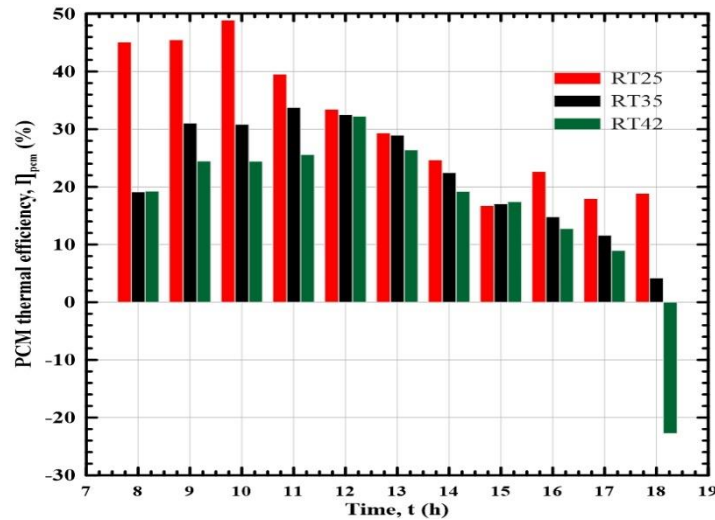


Figure 7. Variation of PCM thermal efficiency with time.

Fig. 7 reveals that RT25 has higher thermal efficiency than RT35 and RT42, which means much heat is absorbed by RT25. The maximum hourly thermal efficiency for RT25 is 48.9% at 10:00 AM, while this value for RT35 is 33.7% one hour later (11:00 AM). RT42 achieves low PCM thermal efficiency as it has the most inferior photocell temperature reduction. Also, the maximum thermal efficiency is achieved at noontime because it takes a long time to melt (due to the high melting range), with a value of 32.2%.

5.1.4. PCM energy storage

Thermal energy inside PCM for the proposed cooling system (PV/HP-PCM) per square meter of photocell area is illustrated in Fig. 8. PCMs are defined as latent storage materials for their proper properties. The PCM is sensibly heated until it melts, where sensible heat storage rises with time. After that, latent heat dominates energy storage. As observed during the first two hours, heat is sensibly absorbed by PCM (small quantity of heat storage); then, the PCM energy storage witnessed a dramatic increase in its value due to the increase in the amount of PCM melted and the intensity of sun rays until noon time. The PCM's temperature rises as more of PCM is converted to the liquid phase, reducing the rate at which heat can be transferred to PCM and, thus, the amount of thermal energy it can store. As shown in Fig. 8 for case RT42, energy storage ended with a negative value because heat flow from the PCM-heat sink in the direction of the photocell via heat pipe, which is not recommended for photocell cooling. The energy storage capacity for RT25 is higher than that of RT42 and RT35 because of the material's proper properties.

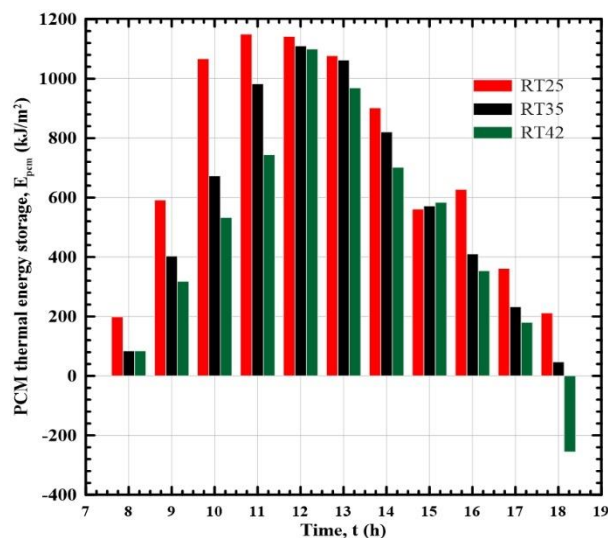


Figure 8. Hourly PCM thermal energy storage.

As clearly shown in Fig. 8, the maximum hourly energy stored for all PCM types is achieved at noontime because the photocell generates much heat (the value of solar intensity is high compared with other times). RT25 achieves maximum energy storage of 1149 kJ/m² compared with 1110 kJ/m² and 1099 kJ/m² for RT35 and RT42, respectively. These findings demonstrate that, depending on the PCM's characteristics and incident solar radiation, the energy stored varies for various PCMs. That reveals that for photocell cooling, PCM selection is essential for maximizing the efficiency and performance of the cooling system.

5.2. Thermal and Electric Performance of the PV/HP-PCM System

5.2.1. Photocell Temperature

Fig. 9 shows the proposed cooling system's effect on photocell temperature using three PCMs, namely RT25, RT35, and RT42. The HP-PCM cooling system reduces the operating temperature of photocells significantly compared to natural cell cooling. Moreover, the PCM type (melting point) substantially impacts the cell's thermal regulation, which decreases the cell temperature by reducing the PCM melting point. The PCM amount has a considerable impact on photocell operating temperature. Since PCMs are defined as latent heat storage materials, the maximum heat is absorbed during the phase change (from liquid to solid during the charging process). In other words, sensible heat is marginal. As a result, the amount of heat transfer from photocell when PCM is in liquid or solid phase is small, leading to high photocell operating temperature, even higher than free photocell cooling. With the increasing PCM amount, the PCM melting takes longer and increases the absorbed heat from the PV panel, decreasing cell temperature. As a result, to ensure thermal regulation for the photocell, the melting period should last until the end of the thermal regulation period. Further increasing the PCM amount, the cooling system impact does not affect temperature reduction compared with the amount required to avoid complete melting before the end of the day, as discussed before in Fig. 6. Hence, it can be stated that the optimal amount of PCM is necessary to last during the thermal regulation period.

Fig. 9 reveals that the maximum photocell temperature is reduced by 8.7 °C for a thickness of 4 cm using RT25. At the same time, RT35 and RT42 decreased the operating temperature of the photocell by 7.5 and 7.3 °C compared with the unmodified photocell at the same PCM thickness, respectively. These results make it worth mentioning that the cooling system effectively reduces the operating temperature of the photocell compared with conventional cell cooling.

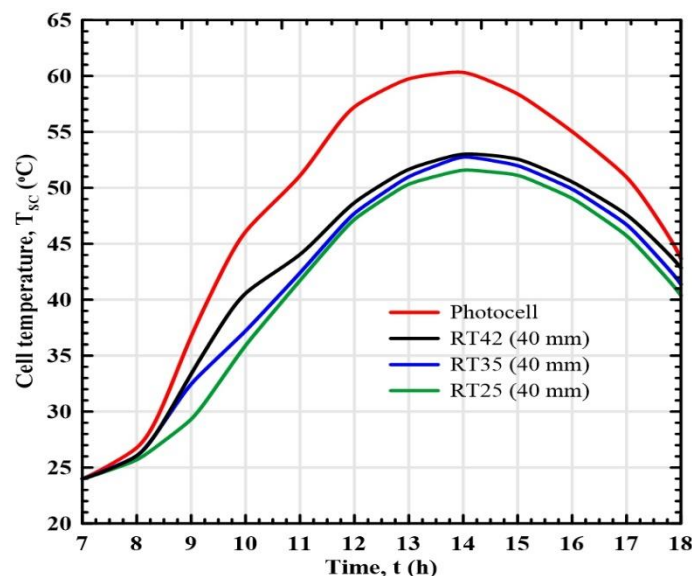


Figure 9. Photocell temperature by using RT42, RT35, RT42, and conventional photocell.

As shown in Fig. 9, it is also important to note that a decrease in the PCM's melting point decreases the photocell's temperature. The current result of the photocell operating temperature is compared with the result of [53]. This comparison shows that the current proposed cooling system reduces the maximum photocell operating temperature using PCM RT25 by 8.7 °C, compared with 8.1 °C for [53] using PCM type RT55. Another comparison of photocell operating temperature with the experimental data of [54] is reported. In their study, PCM RT42 was used in the experiment under summer conditions. They reported that the highest average temperature drop was achieved in July when the PV front surface was reduced by 6.2 °C, 2.2 °C lower than the current study. Finally, Yousef et al. [55] reported that a reduction of 9 °C in operating temperature was achieved when using PCM type TR42 directly attached behind the photocell for summer conditions, 0.3 °C higher than the current results. This previous comparison shows the present cooling system's effectiveness besides the configuration's advantages (indirect PCM cooling).

5.2.2. Photocell electric efficiency

Fig. 10 indicates the variation in photocell electric efficiency for the proposed cooling system versus the traditional photocell for summer. As listed in Eq. (7), the electric efficiency of the photocell is temperature-dependent. As a result, the trend of electric efficiency is inverse to solar radiation. The graph illustrates clearly that the electric efficiency drops from the morning until 14:00. After that, solar intensity and ambient temperature decline, causing a decrease in photocell temperature and increasing electric efficiency.

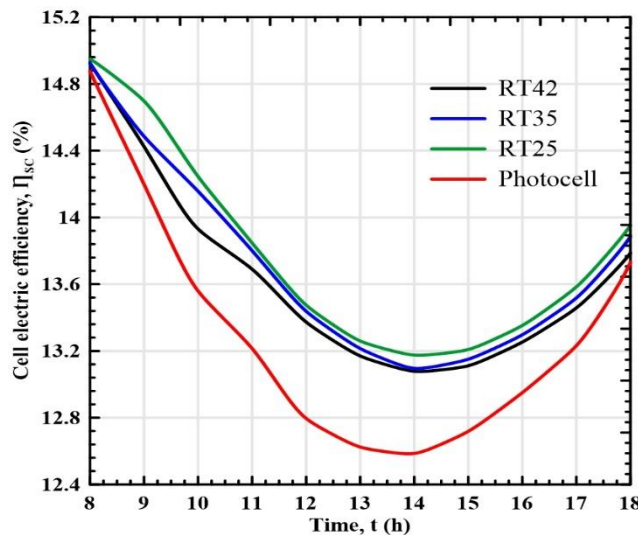


Figure 10. The variation of photocell electric efficiency with time.

The photocell panel employing PCM-RT42, RT35, and RT25 has an electric efficiency improvement of 4.5%, 5.0%, and 5.3% over the standard photocell. This enhancement order is similar to the order of operating temperature of the photocell, as shown in Fig. 9. The current data of average electric efficiency of the photocell are comparable to those of [56] regarding the thermal regulation of the PV with PCM. It is found that the enhancement of the average electrical efficiency of the current work is about 3.6% compared with 5% obtained by [56]. However, in the present work, it is assumed that the photocell has a reference efficiency of 15%, while [56] assumed a reference efficiency of 20%, which means higher operating cell efficiency due to the enhancement in photocell conversion efficiency.

5.2.3. Electric power output

The variation in photocell output power is illustrated in Fig. 11 for unmodified photocell and the proposed cooling system under summer climate. An increase in the temperature of photocell has been proven to reduce the electrical outputs of panels. Photocell power strongly depends on the value of solar radiation, as listed in Eq. (6). As illustrated in Fig. 11, the electricity generation increases with rising

solar intensity till 13:00h. After that, the hybrid system's and conventional photocell's electric power declines.

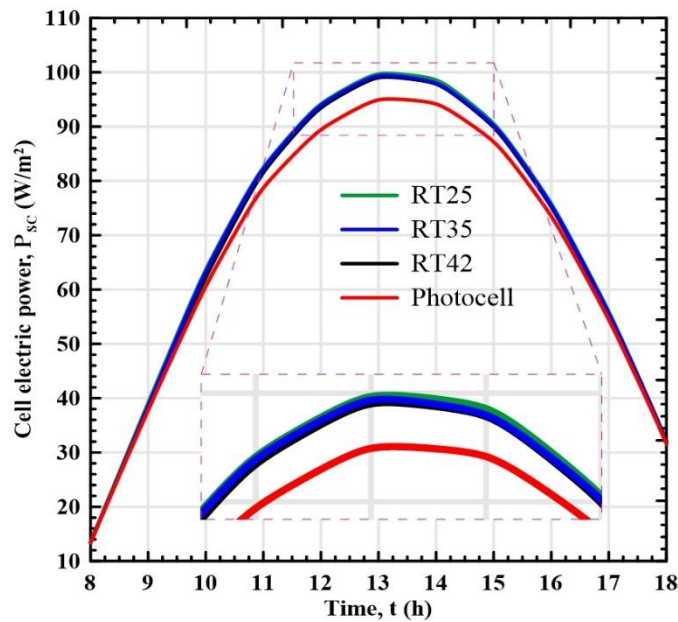


Figure 11. Variation of PV electrical power with time.

The results show that noon is the time when the most electricity is generated. In other words, the photovoltaic system's output power is mostly determined by the intensity of the sun's rays. The electrical power also depends on the photocell operating temperature, as shown in Fig. 11. The output power is higher for PCM with a low melting point than other types. Furthermore, the hybrid cooling system with PCM for all types has a higher electric output than that without HP-PCM cooling (due to the low operating temperature of the hybrid cooling system). RT25 achieves a 5.3% enhancement in electric power compared with 5% and 4.5% in the case of using RT35 and RT42, respectively.

6. CONCLUSION

This work presents an efficient passive cooling system for the thermal management of the photocell by incorporating heat pipes as a heat transfer medium between the photocell and phase change material as a heat sink. PCM type impact on the photocell system's electric and thermal performance is studied for three PCMs (RT42, RT35, and RT25). The main conclusion drawn from the research findings is as follows:

- 1) The photocell performance strongly depends on PCM type (melting point). Decrease in the PCM melting point enhances the hybrid cooling system's thermal and electric performance.
- 2) Using PCM-RT25 as a heat sink reduces the maximum temperature of the photocell by 8.7 °C for a PCM thickness of 4 cm. The PCM types RT35 and RT42 with a high melting point reduce the photocell operating temperature by 7.5 °C and 7.3 °C, respectively.
- 3) The PV/HP-PCM system using RT25 improved the electrical efficiency by 5.3%, compared with the conventionally cooled photocell. While the improvement using RT35 and RT42 is 5% and 4.5%, respectively.
- 4) The hourly thermal efficiency arises with decreasing the PCM melting point with a maximum thermal efficiency of 48.9 %, 33.7%, and 32.2 % for RT25, RT35, and RT42, respectively.

- 5) *This cooling system's efficiency allows for research into its operation in the context of concentration photocells using the optimal PCM combination during the hot and cold seasons.*

Acknowledgment

The authors express their appreciation to the Egyptian Ministry of Higher Education (MoHE) and the Egypt-Japan University of Science and Technology (E-JUST) for sponsoring and supporting this research.

REFERENCES

- [1] Nasser, M, Megahed, TF, Ookawara, S, Hassan, H. Techno-economic assessment of green hydrogen production using different configurations of wind turbines and PV panels. *Journal of Energy Systems* 2022; 6: 560-572. DOI: 10.30521/jes.1132111.
- [2] Soliman, AS, Xu, L, Dong, J, Cheng, P. Numerical investigation of a photovoltaic module under different weather conditions. *Energy Reports* 2022; 8: 1045–1058. DOI: 10.1016/j.egy.2022.10.348.
- [3] Browne, MC, Norton, B, McCormack, SJ. Heat retention of a photovoltaic/thermal collector with PCM. *Solar Energy* 2016; 133: 533–548. DOI: 10.1016/j.solener.2016.04.024.
- [4] Huang, MJ, Eames, PC, Norton, B. Thermal regulation of building-integrated photovoltaics using phase change materials. *International Journal of Heat and Mass Transfer* 2004; 47: 2715–2733. DOI: 10.1016/j.ijheatmasstransfer.2003.11.015.
- [5] Nasef, HA, Hassan, H, Mori, S, Nada, SA. Experimental investigation on the performance of parallel and staggered arrays of PCM energy storage system for PV thermal regulation. *Energy Conversion and Management* 2021; 254: 115143. DOI: 10.1016/j.enconman.2021.115143.
- [6] Wu, SY, Zhang, QL, Xiao, L, Guo, FH. A heat pipe photovoltaic/thermal (PV/T) hybrid system and its performance evaluation. *Energy and Buildings* 2011; 43: 3558–3567. DOI: 10.1016/j.enbuild.2011.09.017.
- [7] Bahaidarah, HMS, Baloch, AAB, Gandhidasan, P. Uniform cooling of photovoltaic panels: A review. *Renewable and Sustainable Energy Reviews* 2016, 57, 1520–1544. DOI: 10.1016/j.rser.2015.12.064.
- [8] Tan, L, Date, A, Fernandes, G, Singh, B, Ganguly, S. Efficiency Gains of Photovoltaic System Using Latent Heat Thermal Energy Storage. *Energy Procedia* 2017; 110: 83–88. DOI: 10.1016/j.egypro.2017.03.110.
- [9] Said, MA, Hassan, H. A study on the thermal energy storage of different phase change materials incorporated with the condenser of air-conditioning unit and their effect on the unit performance. *Energy and Building* 2019; 202. DOI: 10.1016/j.enbuild.2019.109353.
- [10] Soliman, AS, Zhu, S, Xu, L, Dong, J, Cheng, P. Design of an H₂O-LiBr absorption system using PCMs and powered by automotive exhaust gas. *Applied Thermal Engineering* 2021; 191. DOI: 10.1016/j.applthermaleng.2021.116881.
- [11] Ismail, M, Zahra, WK, Ookawara, S, Hassan, H. Boosting the air conditioning unit performance using phase change material: Impact of system configuration. *Journal of Energy Storage* 2022; 56: 105864. DOI: 10.1016/j.est.2022.105864.
- [12] Soliman, AS, Zhu, S, Xu, L, Dong, J, Cheng, P. Melting enhancement of nano-phase change material in cylindrical enclosure using convex/concave dimples: Numerical simulation with experimental validation. *Journal of Energy Storage* 2021; 44. DOI: 10.1016/j.est.2021.103470.
- [13] Zalba, B, Marin, JM, Cabeza, LF, Mehling, H. Review on thermal energy storage with phase change: materials, heat transfer analysis and applications. *Applied Thermal Engineering* 2003; 23: 251-283. DOI: 10.1016/S1359-4311(02)00192-8.
- [14] Kumar, R, Praveen, P, Gupta, S, Saikiran, J, Bharj, RS. Performance evaluation of photovoltaic module integrated with phase change material-filled container with external fins for extremely hot climates. *Journal of Energy Storage* 2020; 32: 101876. DOI: 10.1016/j.est.2020.101876.
- [15] Qasim, MA, Ali, HM, Khan, MN, Arshad, N, Khaliq, D, Ali, Z, Janjua, MM. The effect of using hybrid phase change materials on thermal management of photovoltaic panels – An experimental study. *Solar Energy* 2020; 209: 415–423. DOI: 10.1016/j.solener.2020.09.027.
- [16] Savvakis, N, DIALYNA, E, Tsoutsos, T. Investigation of the operational performance and efficiency of an alternative PV + PCM concept. *Solar Energy* 2020; 211: 1283–1300. DOI: 10.1016/j.solener.2020.10.053.
- [17] Ho, CJ, Chou, WL, Lai, CM. Thermal and electrical performances of a water-surface floating PV integrated with double water-saturated MEPCM layers. *Applied Thermal Engineering* 2016; 94: 122–132. DOI: 10.1016/j.applthermaleng.2015.10.097.

- [18] Mahdi, JM, Mohammed, HI, Talebizadehsardari, P. A new approach for employing multiple PCMs in the passive thermal management of photovoltaic modules. *Solar Energy* 2021; 222: 160–174. DOI: 10.1016/j.solener.2021.04.044.
- [19] Naderi, M, Ziapour, BM, Gendeshmin, MY. Improvement of photocells by the integration of phase change materials and thermoelectric generators (PV-PCM-TEG) and study on the ability to generate electricity around the clock. *Journal of Energy Storage* 2021; 36: 102384. DOI: 10.1016/j.est.2021.102384.
- [20] Sudhakar, P, Santosh, R, Asthalakshmi, B, Kumaresan, G, Velraj, R. Performance augmentation of solar photovoltaic panel through PCM integrated natural water circulation cooling technique. *Renewable Energy* 2021; 172: 1433–1448. DOI: 10.1016/j.renene.2020.11.138.
- [21] Carmona, M, Palacio Bastos, A, García, JD. Experimental evaluation of a hybrid photovoltaic and thermal solar energy collector with integrated phase change material (PVT-PCM) in comparison with a traditional photovoltaic (PV) module. *Renewable Energy* 2021; 172: 680–696. DOI: 10.1016/j.renene.2021.03.022.
- [22] Du, Y, Le, N.C.H, Chen, D, Chen, H, Zhu, Y. Thermal management of solar cells using a nano-coated heat pipe plate: an indoor experimental study. *International Journal of Energy Research* 2017; 41: 867–876. DOI: 10.1002/er.3678.
- [23] Soliman, AMA, Hassan, H, An experimental work on the performance of solar cell cooled by flat heat pipe. *Journal of Thermal Analysis and Calorimetry* 2020. DOI: 10.1007/s10973-020-10102-5.
- [24] Jouhara, H, Szulgowska-Zgrzywa, M Sayegh, MA, Milko, J, Danielewicz, J, Nannou, TK, Lester, SP. The performance of a heat pipe based solar PV/T roof collector and its potential contribution in district heating applications. *Energy* 2017; 136: 117–125. DOI: 10.1016/j.energy.2016.04.070.
- [25] Han, X, Zhao, X, Chen, X. Design and analysis of a concentrating PV/T system with nanofluid based spectral beam splitter and heat pipe cooling. *Renewable Energy* 2020; 162: 55–70. DOI: 10.1016/j.renene.2020.07.131.
- [26] Shittu, S, Li, G, Zhao, X, Zhou, X, Ma, X, Akhlaghi, YG. Experimental study and exergy analysis of photovoltaic-thermoelectric with flat plate micro-channel heat pipe. *Energy Conversion and Management* 2020; 207. DOI: 10.1016/j.enconman.2020.112515.
- [27] Gang, P, Huide, F, Jie, J, Tin-Tai, C, Tao, Z. Annual analysis of heat pipe PV/T systems for domestic hot water and electricity production. *Energy Conversion and Management* 2012; 56: 8–21. DOI: 10.1016/j.enconman.2011.11.011.
- [28] Gang, P, Huide, F, Tao, Z, Jie, J. A numerical and experimental study on a heat pipe PV/T system. *Solar Energy* 2011; 85: 911–921. DOI: 10.1016/j.solener.2011.02.006.
- [29] Weng, Y.C, Cho, H.P, Chang, C.C, Chen, S.L. Heat pipe with PCM for electronic cooling. *Applied Energy* 2011; 88: 1825–1833. DOI: 10.1016/j.apenergy.2010.12.004.
- [30] Krishna, J, Kishore, PS, Solomon, AB. Heat pipe with nano enhanced-PCM for electronic cooling application. *Experimental Thermal and Fluid Science* 2017; 81: 84–92, DOI: 10.1016/j.expthermflusci.2016.10.014.
- [31] Behi, H, Ghanbarpour, M, Behi, M. Investigation of PCM-assisted heat pipe for electronic cooling. *Applied Thermal Engineering* 2016; 127: 1132–1142, <https://doi.org/10.1016/j.applthermaleng.2017.08.109>.
- [32] Putra, N, Sandi, AF, Ariantara, B, Abdullah, N, Indra Mahlia, TM. Performance of beeswax phase change material (PCM) and heat pipe as passive battery cooling system for electric vehicles. *Case Studies in Thermal Engineering* 2020; 21: 100655. DOI: 10.1016/j.csite.2020.100655.
- [33] Behi, X, Karimi, D, Gandoman, FH, Akbarzadeh, M, Khaleghi, S, Kalogiannis, T, Hosen, MS, Jagemont, J, Van Mierlo, J, Berecibar, M. PCM assisted heat pipe cooling system for the thermal management of an LTO cell for high-current profiles. *Case Studies in Thermal Engineering* 2021; 25: 100920. DOI: 10.1016/j.csite.2021.100920..
- [34] Wu, W, Yang, X, Zhang, G, Chen, K, Wang, S. Experimental investigation on the thermal performance of heat pipe-assisted phase change material based battery thermal management system. *Energy Conversion and Management* 2017; 138: 486–492. DOI: 10.1016/j.enconman.2017.02.022.
- [35] Sweidan, A, Ghaddar, N, Ghali, K. Optimized design and operation of heat-pipe photovoltaic thermal system with phase change material for thermal storage. *Journal of Renewable and Sustainable Energy* 2016, 8. DOI: 10.1063/1.4943091.
- [36] Gad, R, Mahmoud, H, Ookawara, S, Hassan, H. Energy , exergy , and economic assessment of thermal regulation of PV panel using hybrid heat pipe-phase change material cooling system. *Journal of Cleaner Production* 2022; 364: 132489, DOI: 10.1016/j.jclepro.2022.132489.
- [37] Saad, A, Xu, L, Dong, J, Cheng, P. A novel heat sink for cooling photovoltaic systems using convex / concave dimples and multiple PCMs. *Applied Thermal Engineering* 2022; 215. DOI: 10.1016/j.applthermaleng.2022.119001.
- [38] Wu, W, Yang, X, Zhang, G, Chen, K, Wang, S. Experimental investigation on the thermal performance of heat pipe-assisted phase change material based battery thermal management system. *Energy Conversion and Management* 2017; 138: 486–492, DOI: 10.1016/j.enconman.2017.02.022.
- [39] Zhou, J, Yi, Q, Wang, Y, Ye, Z. Temperature distribution of photovoltaic module based on finite element simulation. *Solar Energy* 2015; 111: 97–103, DOI: 10.1016/j.solener.2014.10.040.

- [40] Notton, G, Cristofari, C, Mattei, M, Poggi, P. Modelling of a double-glass photovoltaic module using finite differences. *Applied Thermal Engineering* 2005; 25: 2854–2877. DOI: 10.1016/j.applthermaleng.2005.02.008.
- [41] Soliman, AMA, Hassan, H, Ahmed, M, Ookawara, S. A 3d model of the effect of using heat spreader on the performance of photovoltaic panel (PV). *Mathematics and Computers in Simulation* 2018. DOI: 10.1016/j.matcom.2018.05.011.
- [42] Soliman, AMA, Hassan, H, Ookawara, S. An experimental study of the performance of the solar cell with heat sink cooling system. *Energy Procedia* 2019; 162: 127–135. DOI: 10.1016/j.egypro.2019.04.014.
- [43] Zohuri, B. Heat pipe design and technology. Springer 2011. DOI: 10.1201/b10806.
- [44] Hassan, H, Harmand, S. Effect of using nanofluids on the performance of rotating heat pipe. *Applied Mathematical Modelling* 2015; 39: 4445–4462. DOI: 10.1016/j.apm.2014.12.023.
- [45] Gad, R, Mahmoud, H, Ookawara, S, Hassan, H. Evaluation of thermal management of photovoltaic solar cell via hybrid cooling system of phase change material inclusion hybrid nanoparticles coupled with flat heat pipe. *Journal of Energy Storage* 2023; 57: 106–185. DOI: 10.1016/j.est.2022.106185.
- [46] Makki, A, Omer, S, Su, Y, Sabir, H. Numerical investigation of heat pipe-based photovoltaic-thermoelectric generator (HP-PV/TEG) hybrid system. *Energy Conversion and Management* 2016; 112: 274–287. DOI: 10.1016/j.enconman.2015.12.069.
- [47] Churchill, SW, Chu, HHS. Correlating equations for laminar and turbulent free convection from a vertical plate. *International Journal of Heat and Mass Transfer* 1975; 18: 1323–1329. DOI: 10.1016/0017-9310(75)90243-4.
- [48] Soliman, AS, Radwan, A, Xu, L, Dong, J, Cheng, P. Energy harvesting in diesel engines to avoid cold start-up using phase change materials. *Case Studies in Thermal Engineering* 2022; 31. DOI: 10.1016/j.csite.2022.101807.
- [49] Atkin, P, Farid, MM. Improving the efficiency of photovoltaic cells using PCM infused graphite and aluminium fins. *Solar Energy* 2015; 114: 217–228. DOI: 10.1016/j.solener.2015.01.037.
- [50] Soliman, AS, Zhu, S, Xu, L, Dong, J, Cheng, P. Numerical simulation and experimental verification of constrained melting of phase change material in cylindrical enclosure subjected to a constant heat flux. *Journal of Energy Storage* 2021; 35. DOI: 10.1016/j.est.2021.102312.
- [51] Hassan, H, Shafey, NYA. 3D study of convection-radiation heat transfer of electronic chip inside enclosure cooled by heat sink. *International Journal of Thermal Science* 2021; 159: 106–585. DOI: 10.1016/j.ijthermalsci.2020.106585.
- [52] Hassan, H, Abdel Shafey, NY, Uddin, Z, Hawwash, AA. 3D investigation on the impact of chips positions and number on their cooling inside cavity. *Journal of Mechanical Science and Technology* 2021; 35: 5233–5244. DOI: 10.1007/s12206-021-1040-z.
- [53] Nada, SA, El-Nagar, DH, Hussein, HMS. Improving the thermal regulation and efficiency enhancement of PCM-Integrated PV modules using nano particles. *Energy Conversion and Management* 2018; 166: 735–743. DOI: 10.1016/j.enconman.2018.04.035.
- [54] Sharaf, M, Yousef, MS, Huzayyin, AS. Year-round energy and exergy performance investigation of a photovoltaic panel coupled with metal foam/phase change material composite. *Renewable Energy* 2022; 189: 777–789. DOI: 10.1016/j.renene.2022.03.071.
- [55] Yousef, MS, Sharaf, M, Huzayyin, AS. Energy, exergy, economic, and enviroeconomic assessment of a photovoltaic module incorporated with a paraffin-metal foam composite: An experimental study. *Energy* 2022; 238: 121–807. DOI: 10.1016/j.energy.2021.121807.
- [56] Elsheniti, MB, Hemedah, MA, Sorour, MM, El-Maghlany, WM. Novel enhanced conduction model for predicting performance of a PV panel cooled by PCM. *Energy Conversion and Management* 2020; 205: 112–456. DOI: 10.1016/j.enconman.2019.112456.